ORIGINAL ARTICLE

The P2X$_7$ receptor tracer [^{11}C]SMW139 as an *in vivo* marker of neuroinflammation in multiple sclerosis: a first-in man study

Marloes H. J. Hagens[1,2] · Sandeep S. V. Golla[3] · Bieneke Janssen[3] · Danielle J. Vugts[3] · Wissam Beaino[4] ·
Albert D. Windhorst[3] · James O'Brien-Brown[6] · Michael Kassiou[6] · Robert C. Schuit[3] · Lothar A. Schwarte[5] ·
Helga E. de Vries[1,4] · Joep Killestein[1,2] · Frederik Barkhof[1,3,7] · Bart N. M. van Berckel[3] · Adriaan A. Lammertsma[3]

Abstract

Purpose The novel PET tracer [^{11}C]SMW139 binds with high affinity to the P2X$_7$ receptor, which is expressed on pro-inflammatory microglia. The purposes of this first in-man study were to characterise pharmacokinetics of [^{11}C]SMW139 in patients with active relapsing remitting multiple sclerosis (RRMS) and healthy controls (HC) and to evaluate its potential to identify *in vivo* neuroinflammation in RRMS.

Methods Five RRMS patients and 5 age-matched HC underwent 90-min dynamic [^{11}C]SMW139 PET scans, with online continuous and manual arterial sampling to generate a metabolite-corrected arterial plasma input function. Tissue time activity curves were fitted to single- and two-tissue compartment models, and the model that provided the best fits was determined using the Akaike information criterion.

Results The optimal model for describing [^{11}C]SMW139 kinetics in both RRMS and HC was a reversible two-tissue compartment model with blood volume parameter and with the dissociation rate k_4 fixed to the whole-brain value. Exploratory group level comparisons demonstrated an increased volume of distribution (V_T) and binding potential (BP_{ND}) in RRMS compared with HC in normal appearing brain regions. BP_{ND} in MS lesions was decreased compared with non-lesional white matter, and a further decrease was observed in gadolinium-enhancing lesions. In contrast, increased V_T was observed in enhancing lesions, possibly

✉ Marloes H. J. Hagens
m.hagens1@vumc.nl

Sandeep S. V. Golla
s.golla@vumc.nl

Bieneke Janssen
bieneke.janssen@pennmedicine.upenn.edu

Danielle J. Vugts
d.vugts@vumc.nl

Wissam Beaino
w.beaino@vumc.nl

Albert D. Windhorst
ad.windhorst@vumc.nl

James O'Brien-Brown
jobr4491@uni.sydney.edu.au

Michael Kassiou
michael.kassiou@sydney.edu.au

Robert C. Schuit
rc.schuit@vumc.nl

Lothar A. Schwarte
l.schwarte@vumc.nl

Helga E. de Vries
he.devries@vumc.nl

Joep Killestein
j.killestein@vumc.nl

Frederik Barkhof
f.barkhof@vumc.nl

Bart N. M. van Berckel
b.berckel@vumc.nl

Adriaan A. Lammertsma
aa.lammertsma@vumc.nl

Extended author information available on the last page of the article

resulting from disruption of the blood-brain barrier in active MS lesions. In addition, there was a high correlation between parameters obtained from 60- to 90-min datasets, although analyses using 60-min data led to a slight underestimation in regional V_T and BP_{ND} values.

Conclusions This first in-man study demonstrated that uptake of [11C]SMW139 can be quantified with PET using BP_{ND} as a measure for specific binding in healthy controls and RRMS patients. Additional studies are warranted for further clinical evaluation of this novel neuroinflammation tracer.

Keywords Multiple sclerosis · Positron emission tomography · Neuroinflammation · [11C]SMW139 · Purinergic signalling · P2X7-receptor

Introduction

Radiological evaluation of relapsing remitting multiple sclerosis (RRMS) is mainly based on new T2 lesions and active gadolinium-enhancing lesions on magnetic resonance imaging (MRI) [1]. However, detection of these disease-specific lesions by MRI only partly demonstrates the underlying pathophysiological processes in MS. As positron emission tomography (PET) can be used to visualise distinct molecular processes *in vivo*, it may provide unique insights in the pathophysiology of neuroinflammation (and neurodegeneration) in MS [2]. Over the past decades, the translocator protein 18 kDa (TSPO), present on the mitochondrial membrane of microglial cells, has been used as an *in vivo* marker of neuroinflammation in several neurological disorders including MS [3–5]. Although in general results have been positive, the use of TSPO as a marker for neuroinflammation has some limitations, such as an intracellular binding site, genetic polymorphisms, and additional binding sites on monocytes and vascular wall endothelium [6, 7]. In addition, TSPO does not differentiate between resting state and pro-inflammatory and neuro-protective microglia subtypes [8]. Therefore, new PET tracers are needed, which specifically target proteins that reflect the status of microglial cells. Recently, using well-characterised post-mortem tissues of patients with MS and activated human microglia, it has been demonstrated that the purinergic P2X7 receptor is highly expressed on pro-inflammatory microglia and macrophages, is selectively expressed within MS lesions, and may be involved in the neuroinflammatory cascade [8–10]. To a lesser extent, expression of P2X7 receptor has also been found in grey matter on astrocytes, oligodendrocytes, and neurons [11]. Moreover, it was shown that the radioligand [11C]SMW139 selectively binds to the P2X7 receptor with high affinity in preclinical *in vivo* studies and in post-mortem human tissues [8, 12–14].

However, so far, no human *in vivo* data are available for this tracer and its validity to visualise activated microglia and macrophages. The aims of this study were therefore to evaluate *in vivo* pharmacokinetic characteristics of [11C]SMW139 and to perform a proof of concept study assessing whether this novel tracer can be used for identifying neuroinflammation in RRMS.

Material and methods

Subjects

All subjects were recruited between June 2017 and April 2018 from the MS Center of the Amsterdam UMC, location VUmc. Patients were diagnosed with relapsing remitting MS according to the 2017 revisions of the McDonald criteria, and they had active disease at recruitment [15]. Healthy controls were age-matched to the patients. All subjects were screened for relevant neurological, immunological, cardiac, renal, and haematological diseases using medical history, physical and neurological examinations, and blood tests. Patients were not allowed to use immunomodulating medication at the time of the PET-scan, taking into account a washout of 2–4 weeks for first-line treatment, 6–12 weeks for second-line treatment, and 6 weeks for intravenous methylprednisolone.

This study was approved by the Medical Ethics Review Committee of the Amsterdam UMC, location VUmc (2016.548). Written informed consent was obtained from all subjects prior to the first study activity.

MRI scanning protocol

MR imaging was performed on a 3-T General Electric Discovery MR750 system within 7 days of the PET scan. MR imaging included 3D T1 (repetition time 8.2 ms, echo time 3.2 ms, flip angle 12°, measured voxel size 1.0 × 1.0 × 1.0 mm³) for structural information. For patients, a 3D fluid attenuation inversion recovery (FLAIR) (repetition time 8000 ms, echo time 130 ms, inversion time 2340 ms, measured voxel size 1.1 × 1.1 × 1.2 mm³) and a post-contrast SE T1 (repetition time 660 ms, echo time 9 ms, measured voxel size 0.8 × 1.0 × 3.0 mm³) were used for segmentation of the gadolinium-enhancing and non-enhancing MS lesions.

PET scanning protocol

Radiosynthesis of [11C]SMW139 was performed following the procedures described by Janssen et al., with slight modification since K_2CO_3 (5 mg) was used as a base instead of NaOH [12]. The tracer was obtained with a > 98%

radiochemical purity. PET scans were performed on an Ingenuity TF PET-CT scanner (Philips Medical Systems, Best, The Netherlands). Following an automated intravenous infusion of a bolus of 362 ± 44 MBq [^{11}C]SMW139 (molar activity of 59 ± 38 GBq μmol^{-1} at time of injection) a 90-min dynamic PET scan was acquired (see Online Resource 1 for information per subject). Emission data were collected in list mode and reconstructed into a dynamic dataset of 22 frames (1 $\times$ 15, 3 $\times$ 5, 3 $\times$ 10, 4 $\times$ 60, 2 $\times$ 150, 2 $\times$ 300, 7 $\times$ 600 s) using a standard reconstruction algorithm (BLOB-OS-TF) including corrections for scatter, randoms, attenuation, and dead time, and with a final voxel size of $2 \times 2 \times 2$ mm^3.

Input functions

Automated continuous arterial blood sampling from a radial artery cannula was performed at a withdrawal rate of 5 mL min^{-1} for the first 5 min and 2.5 mL min^{-1} for the remainder of the scan. At set times (5, 10, 20, 40, 60, 75, and 90 min), continuous withdrawal was interrupted briefly for the collection of manual arterial blood samples [16]. Manual plasma samples were analysed using high-performance liquid chromatography (HPLC) to determine fractions of intact [^{11}C]SMW139 and its radioactive metabolites, as has been described in more detail before [17]. In brief, plasma supernatant was separated from blood cells and diluted with 2 mL of water and loaded onto an activated tC18 Sep-Pak, followed by washing with 3 mL of water to obtain the polar fraction. The non-polar fraction was then eluted with 2 mL of MeOH and 1 mL of water and further analysed by HPLC. As a stationary phase, a Gemini C18 5-μm (10 $\times$ 250 mm) column with a gradient of acetonitrile (A) and 0.1% DIPA (B) as eluent was used. Metabolite-corrected arterial plasma input functions were obtained by correcting the arterial whole-blood TACs for both plasma to whole-blood ratios, metabolite fraction, and time delay.

Image processing

For the MS patients, T2 lesions were segmented on the FLAIR scans using the automated segmentation tool kNN-TPP [18]. Next, lesion filling of the T1-weighted scans was performed using LEAP [19]. Next, the T1-weighted scans were registered to the summed PET images and this coregistration was then applied to the whole dynamic PET scan. Subsequently, segmentation of grey matter, white matter, and cerebrospinal fluid of the co-registered MRI scans was performed using SPM12 software [20]. PVElab [21] was used for region of interest (ROI) definition according to the Hammers template [22]. By superimposing these ROIs onto the dynamic PET scans, regional time activity curves (TACs) were generated. In addition, cortical grey matter ROIs were combined to define larger cortical ROIs, e.g., frontal cortex, temporal cortex,

and cingulate cortex. Moreover, segmented T2 lesions were subtracted from the white matter mask to define non-lesional white matter. Finally, lesions with gadolinium enhancement on the post-contrast T1-weighted scans were identified on the segmented T2 lesion masks, to obtain a separate mask for enhancing lesions only.

Kinetic modelling

To identify the optimal tracer kinetic model for describing [^{11}C]SMW139 kinetics, standard single-tissue (1T2k) together with reversible and irreversible two-tissue (2T3k and 2T4k, respectively) compartment models was used, both with and without blood volume parameter (V_B). In addition, a dual run 2T4k_V_B model was used in which the first run was used to estimate whole-brain grey and white matter k_4, which subsequently was used to fix k_4 for individual grey and white matter ROIs in the second run (2T4k_V_B_k_4). This analysis was added to reduce the number of fit parameters, thereby improving precision of the other fit parameters. The Akaike information criterion (AIC) was used to compare fits of different models [23]. In addition, reliability of parameter estimates was evaluated using the percentage standard error (%SE) in parameter estimates. For more robust parameters, a %SE cut-off of 25% was used for K_1, k_2, and V_B, and a cut-off of 50% for k_3 and k_4.

Group differences

Differences in volume of distribution (V_T) and binding potential (BP_{ND}, defined as k_3/k_4) derived using the optimal model were used to compare the patient group with the healthy controls. Per subject, ROIs with %SE higher than the cut-off for the various parameters were excluded from this analysis. Exploratory evaluation of the group differences was carried out using an independent t test in SPSS 22.0 (IBM Corp., Armonk, NY).

Scan duration

To evaluate the impact of a shorter scan duration on parameter estimates, analysis was repeated using only 60 min data. Comparisons were performed using linear regression and Bland-Altman analysis.

Results

Cohort description

Demographic information for the subjects included in this study is provided in Table 1, and additional information is available in Online Resource 1. The RRMS patients and

Table 1 Cohort description

	RRMS (n = 5)	HC (n = 5)
Age, mean ± SD (years)	38.6 ± 12.5*	36.6 ± 13.5*
Gender, male/female	2/3	2/3
Disease duration, median and range (years)	0.8 (0.1–5.0)	
EDSS, median and range	3.0 (2.0–5.5)	
T25FW, median and range	4.4 (3.8–8.0)	
9-HPT, median and range	24.4 (16.9–25.7)	
SDMT, median and range	44 (33–57)	
T2 lesion volume, median and range (cm^3)	18.1 (0.5–31.1)	
Volume gadolinium enhancing lesions, median and range (cm^3)	0.7 (0–10.8)	

EDSS Expanded Disability Status Scale, *HC* healthy control, *RRMS* relapsing remitting multiple sclerosis

*Mann-Whitney *U* test: $p = 0.84$

healthy controls were comparable with respect to age and gender. All RRMS patients had a short disease duration, with a median of less than 1 year. All five patients had at least one clinical relapse in the 6 months prior to study participation, with one or more gadolinium-enhancing lesions on the clinical MRI. Three patients where still recovering from a recent relapse at the time of study participation. Four patients had at least one gadolinium-enhancing lesion on the study MRI.

PET image

Figure 1 provides SUV images of one healthy control and one MS patient.

Tracer kinetics

Based on the AIC, pharmacokinetics of [^{11}C]SMW139 were best described by the 2T4k_V$_B$_k$_4$ model. This model was preferred in all subjects, and only in a few ROIs, 2T4k_V$_B$ or 2T3k_V$_B$ was preferred. Figure 2 illustrates a few model fits for the TACs of grey and white matter ROIs of representative patients and controls. These TACs demonstrate fast clearance of [^{11}C]SMW139. Mean micro/macro parameters for all the grey and white matter regions of interest, estimated using the optimal model, are presented in Table 2. The rate of [^{11}C]SMW139 entering the brain, which is expressed by K$_1$, was comparable between patients and controls. However, the rate of efflux from the non-displaceable compartment to the blood, represented by k$_2$, was high, being higher in controls

Fig. 1 An SUV image of one healthy control and one patient

Fig. 2 Model fits. Typical time activity curves (TACs) and corresponding fits obtained using the 2t4k_V_B_k_4 model for the frontal cortex of a healthy control (**a**) and an RRMS patient (**b**), the thalamic grey matter for a healthy control (**c**) and an RRMS patient (**d**), and the non-lesional white matter (**e**) and MS lesions of an MS patient (**f**). Standardized uptake values (SUV) have been calculated as the tissue radioactivity concentration divided by the injected activity per kilogramme of body weight
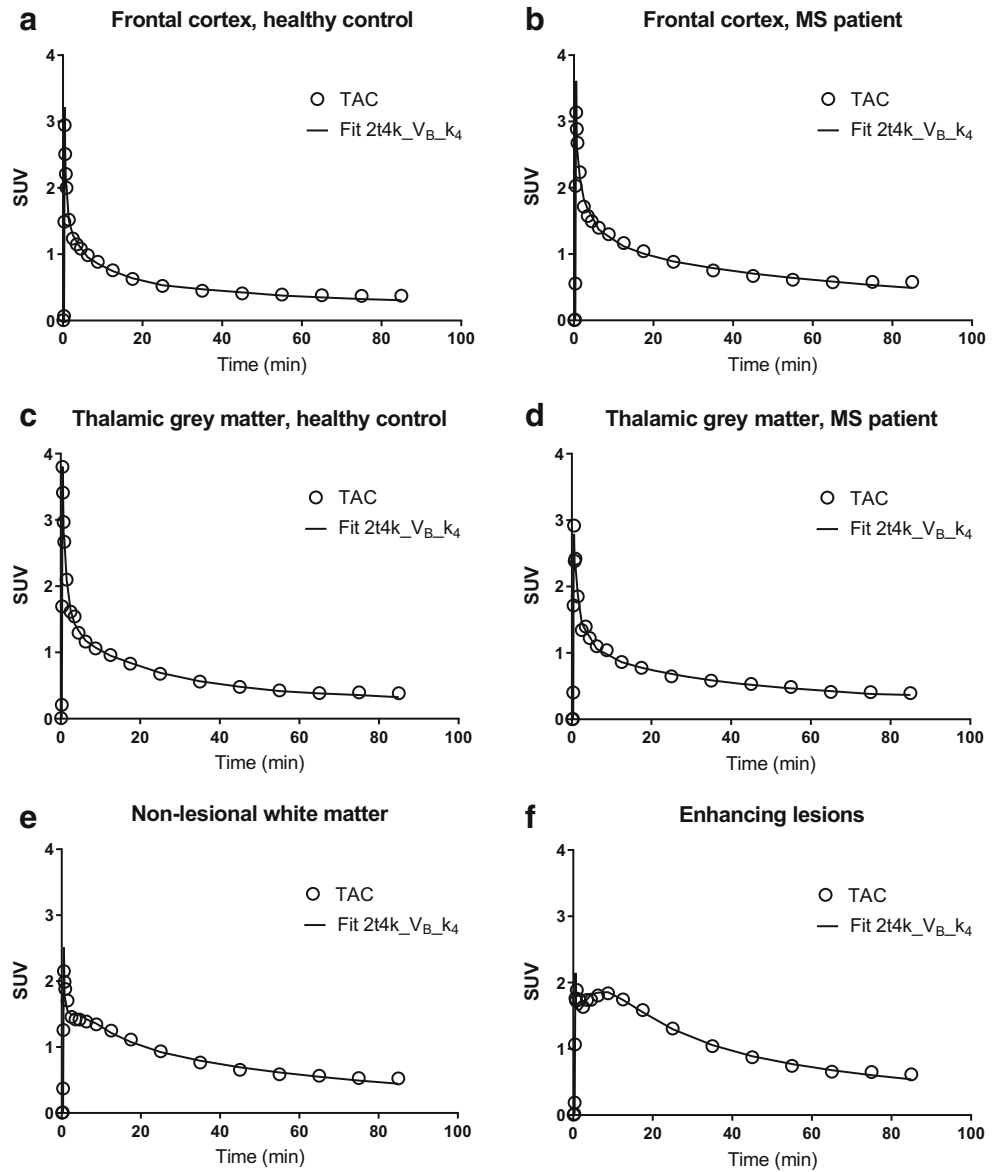
Table 2 Mean parameter estimates 2T4k_V_B_k_4 for whole-brain grey and white matter for all relapsing remitting multiple scleroses (RRMS) patients and healthy controls (HC)

	K_1	k_2	k_3	k_4	V_B
Grey matter					
RRMS	0.087 ± 0.030	0.535 ± 0.115	0.035 ± 0.010	0.020 ± 0.008	0.075 ± 0.019
HC	0.085 ± 0.022	0.686 ± 0.127	0.032 ± 0.012	0.029 ± 0.009	0.075 ± 0.015
p value*	0.44	< 0.001	0.001	0.17	0.83
White matter					
RRMS	0.062 ± 0.025	0.378 ± 0.150	0.043 ± 0.017	0.032 ± 0.012	0.057 ± 0.016
HC	0.062 ± 0.020	0.526 ± 0.146	0.057 ± 0.021	0.058 ± 0.019	0.054 ± 0.012
p value*	0.88	< 0.001	< 0.001	0.041	0.061

HC healthy control, *RRMS* relapsing remitting multiple sclerosis

*Independent t test in SPSS 22.0

Fig. 3 Regional volume of distribution and binding potential. **a** V_T and **b** BP_{ND} values of the five healthy controls (HC) in blue and five multiple sclerosis patients (MS) in red, derived using the 2T4k_V_B_k_4 model, for several grey matter (GM) and white matter (WM) regions of interest. The horizontal blue and red lines represent the mean values for the two subject groups per region. Regions with unreliable parameter estimates (standard deviation for k_3 > 50%) were excluded. Group differences were analysed using an independent t test in SPSS 22.0
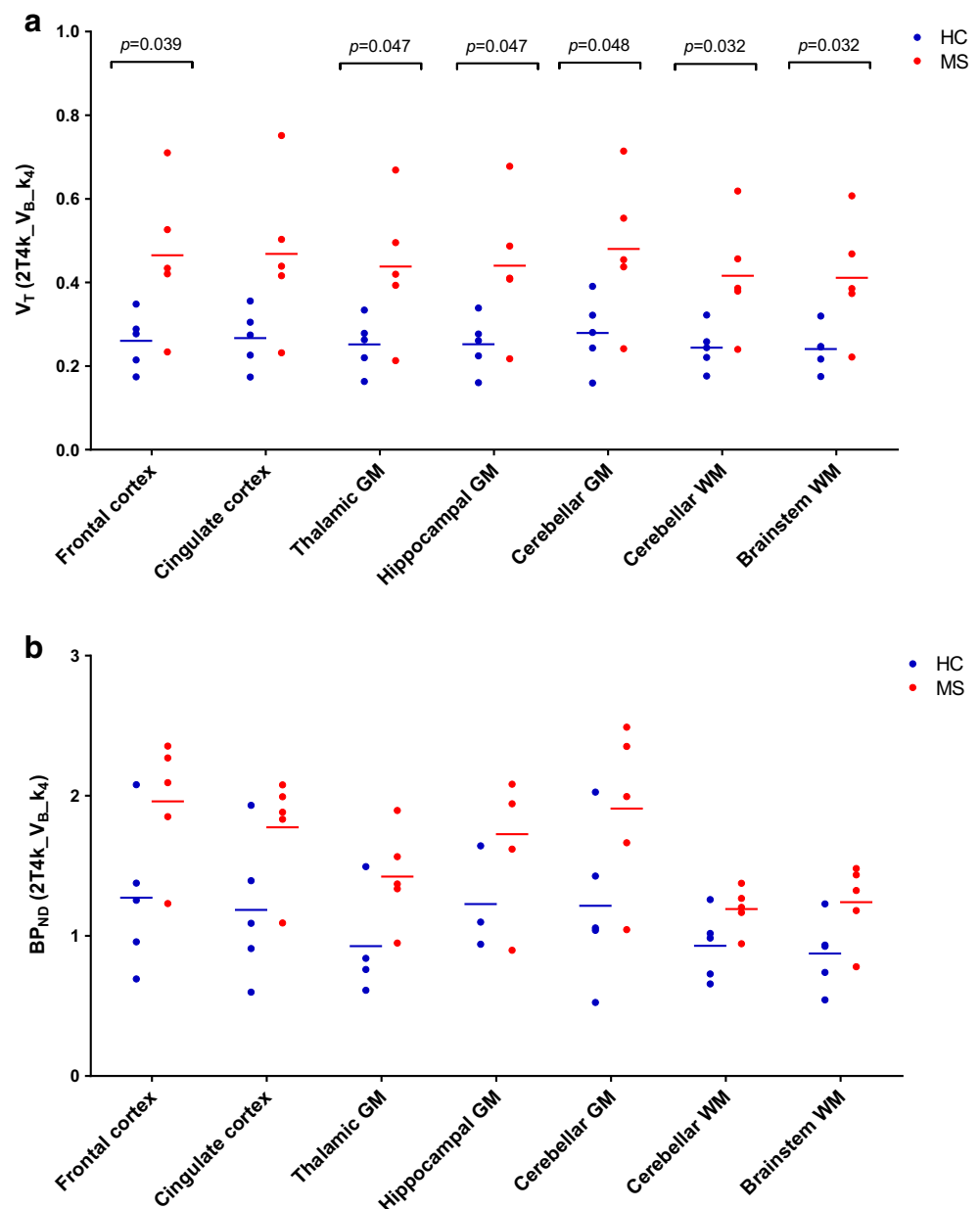
than in patients. In addition, the rate of influx to the specific binding compartment, expressed by k_3, was different between patients and controls, but small in both groups. This rapid clearance from the non-displaceable compartment combined with a low rate of specific binding resulted in a small specific compartment for [^{11}C]SMW139. This made kinetic parameter estimation for this specific compartment prone to noise, resulting in unreliable k_4 estimates in smaller ROIs (data not shown). Fixing k_4 to within-subject whole-brain grey and white matter values (2T4k_V_B_k_4 model) improved reliability of the model estimates. As Online Resource 2 shows, the %SE for 2T4k_V_B_k_4 parameter estimates were low, except for very few ROIs.

Group differences

V_T and BP_{ND} values for the various ROIs are presented in Fig. 3 a and b, respectively. For all regions, mean V_T and BP_{ND} were higher for patients than for controls. For V_T, this group difference was statistically significant (p = 0.032–0.048), except for cingulate cortex (p = 0.055). It should be noted that when these pilot results were corrected for multiple testing (i.e., after Bonferroni correction p < 0.007 would be considered significant); the group differences did not reach statistical significance. For BP_{ND}, the group difference did not reach statistical significance for any of the ROIs.

Due to unreliable parameter estimates, as illustrated in Online Resource 2, one healthy control was not included in the thalamic grey matter and two healthy controls were excluded from the hippocampal grey matter. The figures on group differences including these subject are presented in Online Resource 3.

Multiple sclerosis lesions

Four patients showed gadolinium-enhancing lesions, but in the patient with the smallest enhancing lesion, the corresponding TAC was too noisy, resulting in unreliable kinetic parameter estimates (subject MS2). Results for the other three subjects are presented in Fig. 4. As Fig. 4a illustrates, mean BP_{ND} decreased in T2 lesions compared with non-lesional white matter. A further decrease was seen in gadolinium-enhancing lesions. In contrast, mean V_T was similar for non-lesional white matter and T2 lesions and increased in enhancing lesions (Fig. 4b). In addition, as the blood-brain barrier is disrupted in active MS lesions, the K_1/k_2 ratio was, as expected, not constant, also showing an increase in enhancing lesions (Fig. 4c).

Impact of scan duration

Regional V_T and BP_{ND} values derived from the 60-min data were compared with those from the 90-min data. Figure 5 a

shows a very strong correlation for both macro parameters for the combined ROIs, with correlation coefficients (R^2) of 0.992 for V_T and 0.986 for BP_{ND}. The slopes indicate an underestimation in the values obtained for the 60-min data, approximately 10% for V_T and 15% for BP_{ND}. Similar results are produces by Bland-Altman analysis. As this underestimation predominantly affected higher parameter values, lower regional group differences were seen for the 60-min data than for the 90 min data, as illustrated in Online Resource 4.

Figure 5 b shows a similar correlation coefficient for V_T and BP_{ND} between the two scan durations for the T2 lesions and the gadolinium-enhancing lesions. Just as for the 90-min data, lesions showed lower BP_{ND} than non-lesional brain tissue for the 60-min data as well.

Discussion

This study shows that binding of $[^{11}C]SMW139$ to the $P2X_7$ receptor tracer can be quantified using a two-tissue reversible plasma input model with fixed k_4. Using this model, it was possible to identify neuroinflammation in both MS lesions and normal appearing brain tissue in RRMS.

In this study, simplified reference tissue models were not evaluated, as the pathophysiology of MS violates the assumptions underlying such models. Firstly, because of global low-grade inflammation in the MS brain, none of the brain regions
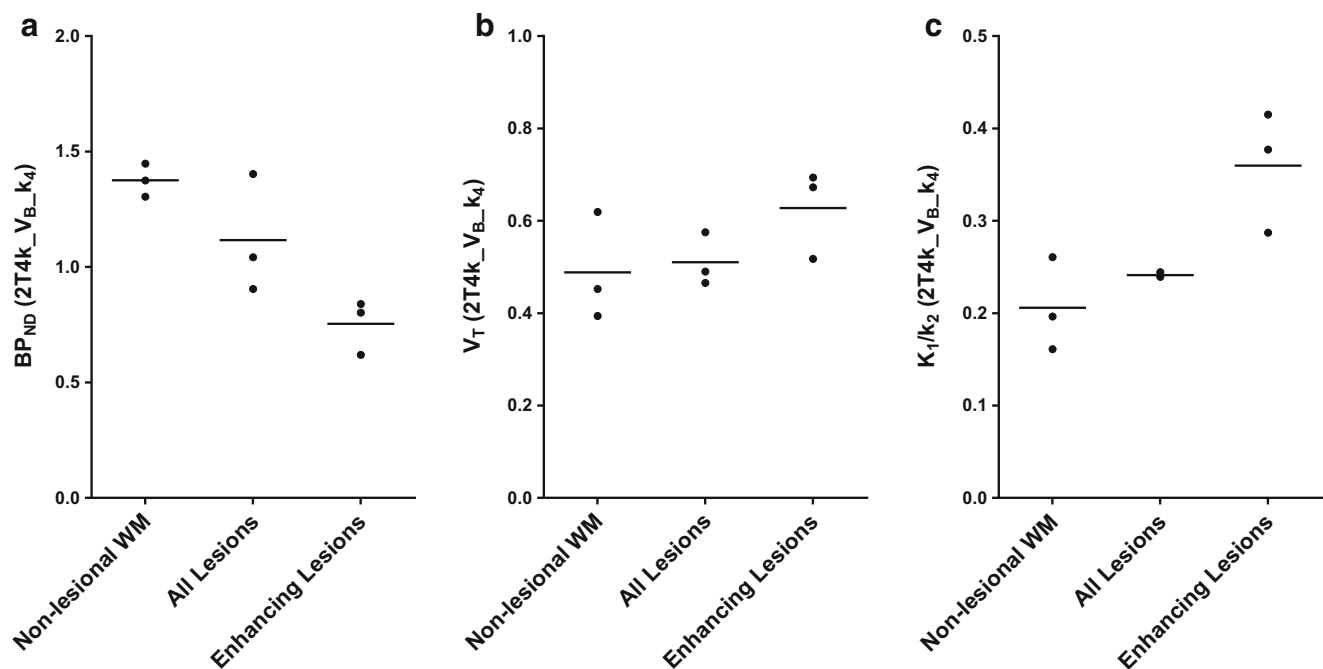
Fig. 4 Kinetic parameters for multiple sclerosis lesions. Lesional and non-lesional 2T4k_V_B_k_4 derived **a** BP_{ND}, **b** V_T, and **c** K_1/k_2 for the three relapsing remitting multiple sclerosis patients with analysable gadolinium-enhancing lesions. Mean BP_{ND} was decreased in T2

lesions, and a further decrease was seen in enhancing lesions, whereas for V_T, an increase was observed. For the K_1/k_2 ratio, an even larger increase was observed in the enhancing lesions, most likely due to disruption of the blood-brain barrier in these active lesions

Fig. 5 Comparison of the 60-min and 90-min datasets. Linear regression for both **a** V_T and **b** BP_{ND} for the combined ROIs showed a very strong correlation between 60- and 90-min datasets. For V_T, there was a systematic underestimation of approximately 10% when reducing scan duration to 60 min; for BP_{ND} this was about 15%. Linear regression for the T2 lesions and gadolinium-enhancing lesions demonstrated an equally strong correlation for (**c**) V_T and (**d**) BP_{ND}. Additional Bland-Altman analysis for the combined ROIs (**e**) V_T and (**e**) BP_{ND} confirms the results from the linear regression analysis
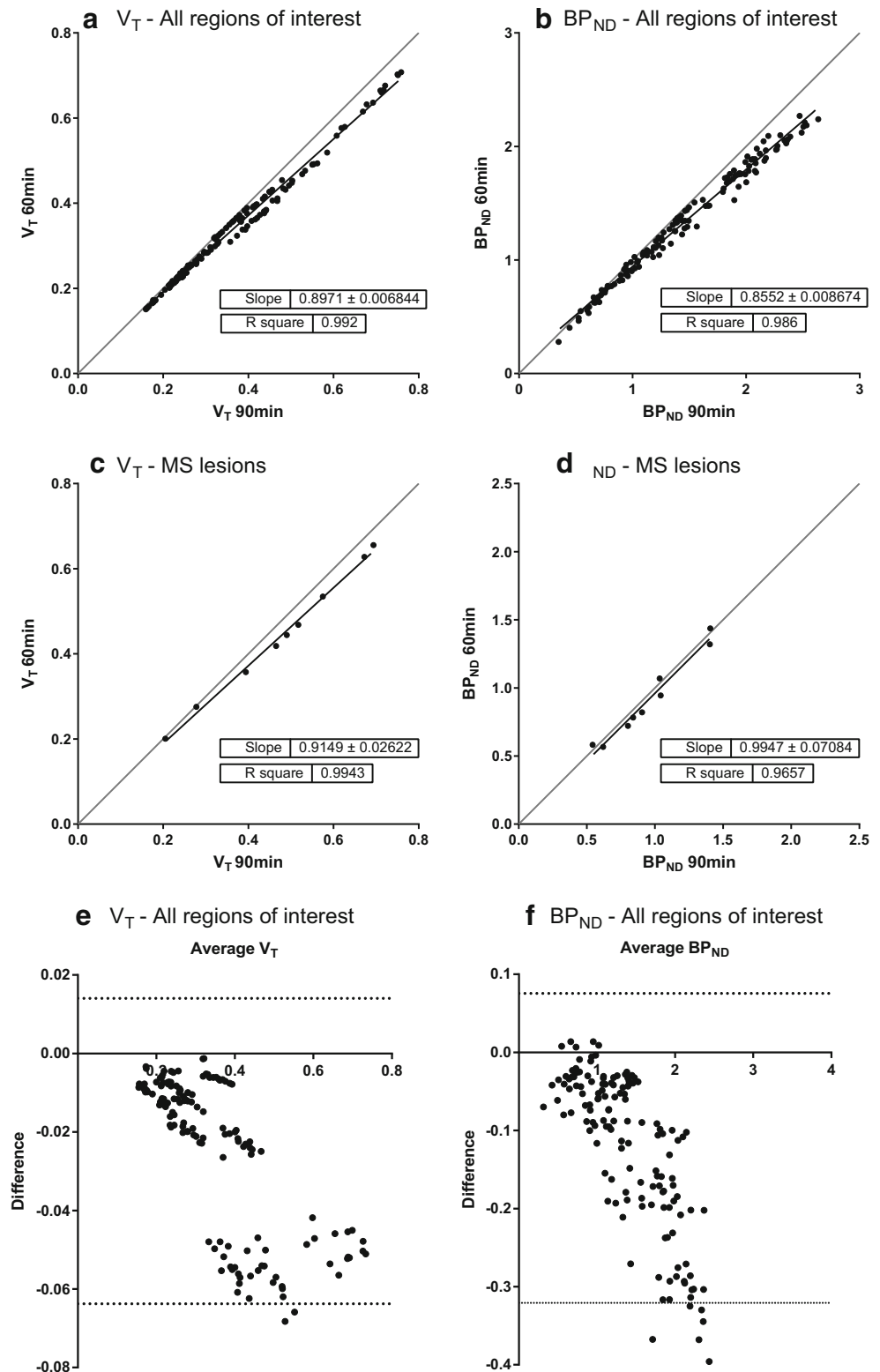
are devoid of specific binding (P2X$_7$ receptors) and hence cannot be considered a reference region [24]. Secondly, due to disruption of the blood-brain barrier in MS, a constant K_1/k_2 across the brain cannot be guaranteed [25].

The rate of influx of [^{11}C]SMW139 from plasma into the brain was sufficient for accurate data analysis. Regional TACs demonstrated fast efflux of [^{11}C]SMW139, which is support-ed by high k_2 estimates. Rapidly declining activity in non-

displaceable and, consequently, specific compartments was observed, resulting in unreliable estimates especially k_4 in smaller ROIs. As $k_4 = k_{off}$, it should be constant for the $P2X_7$ receptor independent of its location. This limited inter-subject variation for k_4 for the different ROIs enabled fixing this parameter for smaller regions to the more reliable whole-brain values. By reducing the number of fit parameters, the precision of the other fit parameters was improved, resulting in acceptable SEs for all estimated parameters in most ROIs when using the $2T4k\_V_B\_k_4$ model.

As demonstrated in Table 2, K_1 was similar in patient and control groups, but k_2 was lower in patients, leading to a higher non-displaceable distribution volume (V_{ND}) in patients. Nevertheless, apart from V_T, BP_{ND} ($= k_3/k_4$) was also higher in patients than in controls, suggesting higher specific binding in the patient group than in the controls for both grey and white matter. This implies an increase in activated microglia in normal appearing brain tissue of these clinically active RRMS patients.

The patient who had the lowest BP_{ND} within the patient group for all ROIs had slightly different demographics: longest disease duration (5 years), highest Expanded Disability Status Scale (5.5), slowest timed 25-foot walk (8.0 s), second slowest 9-Hole Peg Test (25.4 s), lowest Symbol Digits Modalities Test (33 correct), and highest T2 lesion load (31.3 cm^2) with only one small gadolinium-enhancing lesions (0.7 cm^2). This implies that in this patient MS was more progressed compared with the rest of the group, which in turn could result in less active neuroinflammation and therefore lower $P2X_7$ receptor binding [26]. When looking at the demographics of the healthy control with the highest regional BP_{ND} values, this subject's relatively high age stands out (59.2 years). This could resemble an effect of age on $P2X_7$ receptor binding similar to the effect of age on TSPO binding [27], although this clearly needs to be confirmed in a larger cohort.

In the subjects with gadolinium-enhancing lesions, V_T was similar for non-lesional white matter and T2 lesions, but increased in the enhancing lesions. In contrast, BP_{ND} values decreased in T2 lesions, with a further decrease in enhancing lesions. As V_T includes both non-displaceable and specific compartments (the latter represented by BP_{ND}), this indicates that decreased specific binding of [^{11}C]SMW139 was compensated by an increased non-displaceable compartment (non-specifically bound or free tracer). This was reflected by an increase in the K_1/k_2 ratio in these gadolinium-enhancing lesions. The most likely explanation for this increased K_1/k_2 ratio is disruption of the blood-brain barrier in active MS lesions, resulting in increased vascular permeability. Consequently, to quantify [^{11}C]SMW139 binding in these active lesions, BP_{ND} is required.

Interestingly, cerebral [^{11}C]SMW139 BP_{ND} was increased in RRMS patients compared with healthy controls, but counterintuitively specific binding was decreased in active MS lesions. An explanation for this could be found in the heterogeneity of neuroinflammation in MS. Microglia activation is a complex and dynamic process, and different microglia subtypes and macrophages could be involved in both focal and diffuse neuroinflammation [28].

As carbon-11 has a half-life of 20 min, minimal radioactivity is present in both tissue and blood in the final stage of a 90-min scan. Together with the observed fast kinetics of [^{11}C]SMW139, this makes accurate measurements towards the end of the 90-min scans difficult. In addition, a 90-min scan can be quite challenging for both healthy controls and especially patients. Therefore, reducing the scan duration would be beneficial. As shown in Fig. 5, both V_T and BP_{ND} obtained from 60-min datasets correlated very strongly with those from 90-min datasets, despite a slight (systematic) underestimation, suggesting that 60-min scans may be sufficient to assess in vivo kinetics of [^{11}C]SMW139 without compromising quantitative accuracy (see Online Resource 3). In addition, there appeared to be two clusters in the Bland-Altman analysis of V_T. These clusters, however, were not present in the Bland-Altman plot of BP_{ND}. This suggests that the two clusters may be due to differences in non-specific binding.

As this is a first in-man study, the sample size is rather limited, which is the main limitation of this study. Larger study cohorts are needed to confirm these initial findings. In addition, the small sample size resulted in some demographic differences between patient and control groups, even though they did not reach statistical significance. A possible group difference that could be relevant is the number of smokers, as an effect of smoking on neuroinflammation (in MS) has been reported [29–31]. If and how this could impact in vivo [^{11}C]SMW139 binding is currently uncertain.

Moreover, a larger sample size would allow for an assessment of possible correlations between [^{11}C]SMW139 binding and disease duration, clinical outcome measures such as the EDSS- and MRI-derived outcome measures like atrophy. In addition, [^{11}C]SMW139 could potentially be used for longitudinal analyses, which would require additional studies such as test-retest evaluation.

To conclude, this first in-man study demonstrates that a reversible two-tissue plasma input model with fixed k_4 is the preferred model to quantify [^{11}C]SMW139 in healthy controls and RRMS patients.

Additional studies are warranted to further evaluate its clinical relevance as a novel neuroinflammation tracer.

Innovation (GMSI) research grant provided by Merck KGaA (Darmstadt, Germany) and the Dutch MS Research Foundation (programme grant 14-358e).

References

1. Wattjes MP, Rovira A, Miller D, Yousry TA, Sormani MP, de Stefano MP, et al. Evidence-based guidelines: MAGNIMS consensus guidelines on the use of MRI in multiple sclerosis–establishing disease prognosis and monitoring patients. Nat Rev Neurol. 2015;11(10):597–606. https://doi.org/10.1038/nrneurol.2015.157.

2. Hogel H, Rissanen E, Vuorimaa A, Airas L. Positron emission tomography imaging in evaluation of MS pathology in vivo. Mult Scler. 2018;1352458518791680. https://doi.org/10.1177/1352458518791680.

3. Colasanti A, Guo Q, Muhlert N, Giannetti P, Onega M, Newbould RD, et al. In vivo assessment of brain white matter inflammation in multiple sclerosis with (18)F-PBR111 PET. J Nucl Med. 2014;55(7):1112–8. https://doi.org/10.2967/jnumed.113.135129.

4. Giannetti P, Politis M, Su P, Turkheimer FE, Malik O, Keihaninejad S, et al. Increased PK11195-PET binding in normal-appearing white matter in clinically isolated syndrome. Brain. 2015;138(Pt 1):110–9. https://doi.org/10.1093/brain/awu331.

5. Vowinckel E, Reutens D, Becher B, Verge G, Evans A, Owens T, et al. PK11195 binding to the peripheral benzodiazepine receptor as a marker of microglia activation in multiple sclerosis and experimental autoimmune encephalomyelitis. J Neurosci Res. 1997;50(2):345–53. https://doi.org/10.1002/(SICI)1097-4547(19971015)50:2<345::AID-JNR22>3.0.CO;2-5.

6. Rizzo G, Veronese M, Tonietto M, Zanotti-Fregonara P, Turkheimer FE, Bertoldo A. Kinetic modeling without accounting for the vascular component impairs the quantification of [(11)C]PBR28 brain PET data. J Cereb Blood Flow Metab. 2014;34(6):1060–9. https://doi.org/10.1038/jcbfm.2014.55.

7. Banati RB, Newcombe J, Gunn RN, Cagnin A, Turkheimer F, Heppner F, et al. The peripheral benzodiazepine binding site in the brain in multiple sclerosis: quantitative in vivo imaging of microglia as a measure of disease activity. Brain. 2000;123(Pt 11):2321–37.

8. Beaino W, Janssen B, Kooij G, van der Pol SMA, van Het Hof B, van Horssen J, et al. Purinergic receptors P2Y12R and P2X7R: potential targets for PET imaging of microglia phenotypes in multiple sclerosis. J Neuroinflammation. 2017;14(1):259. https://doi.org/10.1186/s12974-017-1034-z.

9. Bhattacharya A, Neff RA, Wickenden AD. The physiology, pharmacology and future of P2X7 as an analgesic drug target: hype or promise? Curr Pharm Biotechnol. 2011;12(10):1698–706.

10. Monif M, Burnstock G, Williams DA. Microglia: proliferation and activation driven by the P2X7 receptor. Int J Biochem Cell Biol. 2010;42(11):1753–6. https://doi.org/10.1016/j.biocel.2010.06.021.

11. Burnstock G. P2X ion channel receptors and inflammation. Purinergic Signal. 2016;12(1):59–67. https://doi.org/10.1007/s11302-015-9493-0.

12. Janssen B, Vugts DJ, Wilkinson SM, Ory D, Chalon S, Hoozemans JJM, et al. Identification of the allosteric P2X7 receptor antagonist [(11)C]SMW139 as a PET tracer of microglial activation. Sci Rep. 2018;8(1):6580. https://doi.org/10.1038/s41598-018-24814-0.

13. Ory D, Celen S, Gijsbers R, Van Den Haute C, Postnov A, Koole M, et al. Preclinical evaluation of a P2X7 receptor-selective radiotracer: PET studies in a rat model with local overexpression of the human P2X7 receptor and in nonhuman primates. J Nucl Med. 2016;57(9):1436–41. https://doi.org/10.2967/jnumed.115.169995.

14. Wilkinson SM, Barron ML, O'Brien-Brown J, Janssen B, Stokes L, Werry EL, et al. Pharmacological evaluation of novel bioisosteres of an adamantanyl benzamide P2X7 receptor antagonist. ACS Chem Neurosci. 2017;8(11):2374–80. https://doi.org/10.1021/acschemneuro.7b00272.

15. Thompson AJ, Banwell BL, Barkhof F, Carroll WM, Coetzee T, Comi G, et al. Diagnosis of multiple sclerosis: 2017 revisions of the McDonald criteria. Lancet Neurol. 2018;17(2):162–73. https://doi.org/10.1016/S1474-4422(17)30470-2.

16. Boellaard R, van Lingen A, van Balen SC, Hoving BG, Lammertsma AA. Characteristics of a new fully programmable blood sampling device for monitoring blood radioactivity during PET. Eur J Nucl Med. 2001;28(1):81–9.

17. Golla SS, Boellaard R, Oikonen V, Hoffmann A, van Berckel BN, Windhorst AD, et al. Quantification of [18F]DPA-714 binding in the human brain: initial studies in healthy controls and Alzheimer's disease patients. J Cereb Blood Flow Metab. 2015;35(5):766–72. https://doi.org/10.1038/jcbfm.2014.261.

18. Steenwijk MD, Pouwels PJ, Daams M, van Dalen JW, Caan MW, Richard E, et al. Accurate white matter lesion segmentation by k nearest neighbor classification with tissue type priors (kNN-TTPs). Neuroimage Clin. 2013;3:462–9. https://doi.org/10.1016/j.nicl.2013.10.003.

19. Chard DT, Jackson JS, Miller DH, Wheeler-Kingshott CA. Reducing the impact of white matter lesions on automated measures of brain gray and white matter volumes. J Magn Reson Imaging. 2010;32(1):223–8. https://doi.org/10.1002/jmri.22214.

20. Ashburner J, Friston KJ. Unified segmentation. Neuroimage. 2005;26(3):839–51. https://doi.org/10.1016/j.neuroimage.2005.02.018.

21. Svarer C, Madsen K, Hasselbalch SG, Pinborg LH, Haugbol S, Frokjaer VG, et al. MR-based automatic delineation of volumes of interest in human brain PET images using probability maps. Neuroimage. 2005;24(4):969–79. https://doi.org/10.1016/j.neuroimage.2004.10.017.

22. Hammers A, Allom R, Koepp MJ, Free SL, Myers R, Lemieux L, et al. Three-dimensional maximum probability atlas of the human

brain, with particular reference to the temporal lobe. Hum Brain Mapp. 2003;19(4):224–47. https://doi.org/10.1002/hbm.10123.

23. Akaike H. A new look at the statistical model identification. IEEE Trans Autom Control. 1974;19(6):716–23.

24. Salinas CA, Searle GE, Gunn RN. The simplified reference tissue model: model assumption violations and their impact on binding potential. J Cereb Blood Flow Metab. 2015;35(2):304–11. https://doi.org/10.1038/jcbfm.2014.202.

25. Folkersma H, Boellaard R, Vandertop WP, Kloet RW, Lubberink M, Lammertsma AA, et al. Reference tissue models and blood-brain barrier disruption: lessons from (R)-[11C]PK11195 in traumatic brain injury. J Nucl Med. 2009;50(12):1975–9. https://doi.org/10.2967/jnumed.109.067512.

26. Lassmann H, van Horssen J, Mahad D. Progressive multiple sclerosis: pathology and pathogenesis. Nat Rev Neurol. 2012;8(11):647–56. https://doi.org/10.1038/nrneurol.2012.168.

27. Schuitemaker A, van der Doef TF, Boellaard R, van der Flier WM, Yaqub M, Windhorst AD, et al. Microglial activation in healthy aging. Neurobiol Aging. 2012;33(6):1067–72. https://doi.org/10.1016/j.neurobiolaging.2010.09.016.

28. Hemmer B, Kerschensteiner M, Korn T. Role of the innate and adaptive immune responses in the course of multiple sclerosis. Lancet Neurol. 2015;14(4):406–19. https://doi.org/10.1016/S1474-4422(14)70305-9.

29. Brody AL, Hubert R, Enoki R, Garcia LY, Mamoun MS, Okita K, et al. Effect of cigarette smoking on a marker for neuroinflammation: a [(11)C]DAA1106 positron emission tomography study. Neuropsychopharmacology. 2017;42(8):1630–9. https://doi.org/10.1038/npp.2017.48.

30. Gao Z, Nissen JC, Ji K, Tsirka SE. The experimental autoimmune encephalomyelitis disease course is modulated by nicotine and other cigarette smoke components. PLoS One. 2014;9(9):e107979. https://doi.org/10.1371/journal.pone.0107979.

31. Alrouji M, Manouchehrinia A, Gran B, Constantinescu CS. Effects of cigarette smoke on immunity, neuroinflammation and multiple sclerosis. J Neuroimmunol. 2019;329:24–34. https://doi.org/10.1016/j.jneuroim.2018.10.004.

Affiliations

Marloes H. J. Hagens[1,2] · Sandeep S. V. Golla[3] · Bieneke Janssen[3] · Danielle J. Vugts[3] · Wissam Beaino[4] · Albert D. Windhorst[3] · James O'Brien-Brown[6] · Michael Kassiou[6] · Robert C. Schuit[3] · Lothar A. Schwarte[5] · Helga E. de Vries[1,4] · Joep Killestein[1,2] · Frederik Barkhof[1,3,7] · Bart N. M. van Berckel[3] · Adriaan A. Lammertsma[3]

[1] MS Center Amsterdam, Amsterdam Neuroscience, Amsterdam UMC - location VUmc, De Boelelaan 1117, 1081, HV Amsterdam, The Netherlands

[2] Department of Neurology, Amsterdam Neuroscience, Amsterdam UMC - location VUmc, De Boelelaan 1117, 1081 HV, Amsterdam, The Netherlands

[3] Department of Radiology and Nuclear Medicine, Amsterdam Neuroscience, Amsterdam UMC - location VUmc, De Boelelaan 1117, 1081, HV Amsterdam, The Netherlands

[4] Department of Molecular Cell Biology and Immunology, Amsterdam UMC - location VUmc, De Boelelaan 1117, 1081, HV Amsterdam, The Netherlands

[5] Department of Anaesthesiology, Amsterdam UMC - location VUmc, De Boelelaan 1117, 1081 HV, Amsterdam, The Netherlands

[6] School of Chemistry, University of Sydney, Sydney, Australia

[7] Institutes of Neurology and Healthcare Engineering, UCL Institute of Neurology, London, UK